Supplementary information

Small heterodimer partner protects against osteoarthritis by inhibiting IKKβ/NF-κB-mediated matrix-degrading enzymes in chondrocytes

Eun-Jung Kang, Jung-Ran Noh, Jae-Hoon Kim, Ji Ah Park, Jeong-Pin Ahn, Min-Chan Kim, Jung Hyeon Choi, Young-Keun Choi, In-Bok Lee, Dong-Hee Choi, Yun Jeong Seo, Yoon Seok Jung, Kyoung-Shim Kim, Jung Hwan Hwang, Yong-Bum Kim, Jong-Soo Lee, Bon Jeong Ku, Jin-Ok Jeong, Hueng-Sik Choi, Jinhyun Kim, Yong-Hoon Kim, and Chul-Ho Lee

Supplementary Figures 1–18 & Legends

Supplementary Tables 1–4

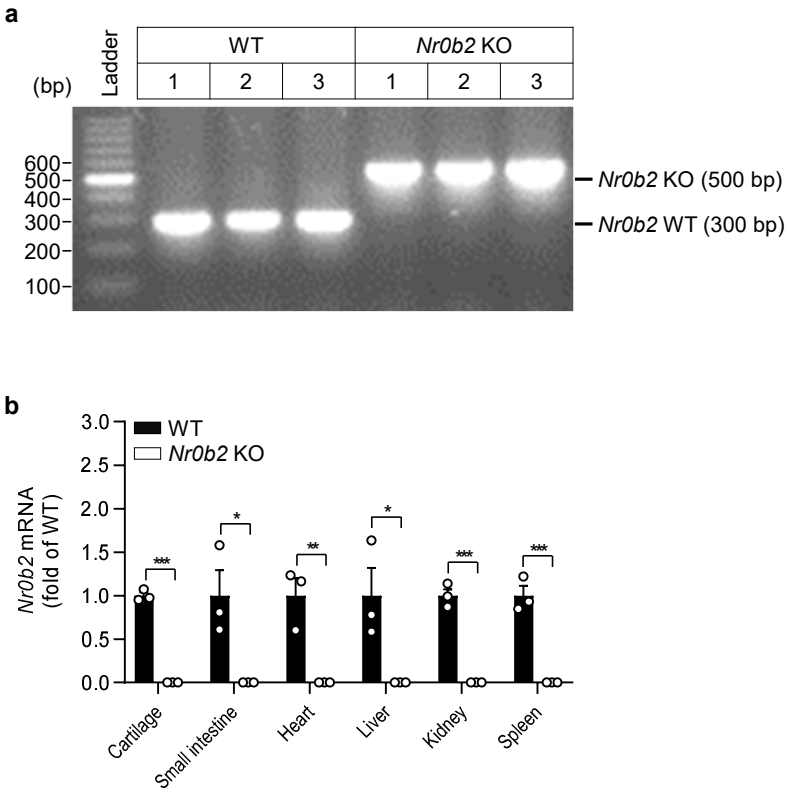

Supplementary Fig. 1 Genotyping of WT and *Nr0b2* KO mice. a Genotyping of WT and *Nr0b2* KO mice was performed by PCR and agarose gel electrophoresis. **b** RT-qPCR results showing the relative mRNA expression levels of *Nr0b2* in different tissues of WT and *Nr0b2* KO mice (n = 3 biologically independent mice per group). Data are presented as means ± SEMs. Statistical analyses were performed using a two-sided Student's t-test (**b**) (*p < 0.05, **p < 0.01, and ***p < 0.001). Source data, including the exact p-values are provided as a Source Data file. The uncropped agarose gel images are provided in Supplementary Fig. 15.

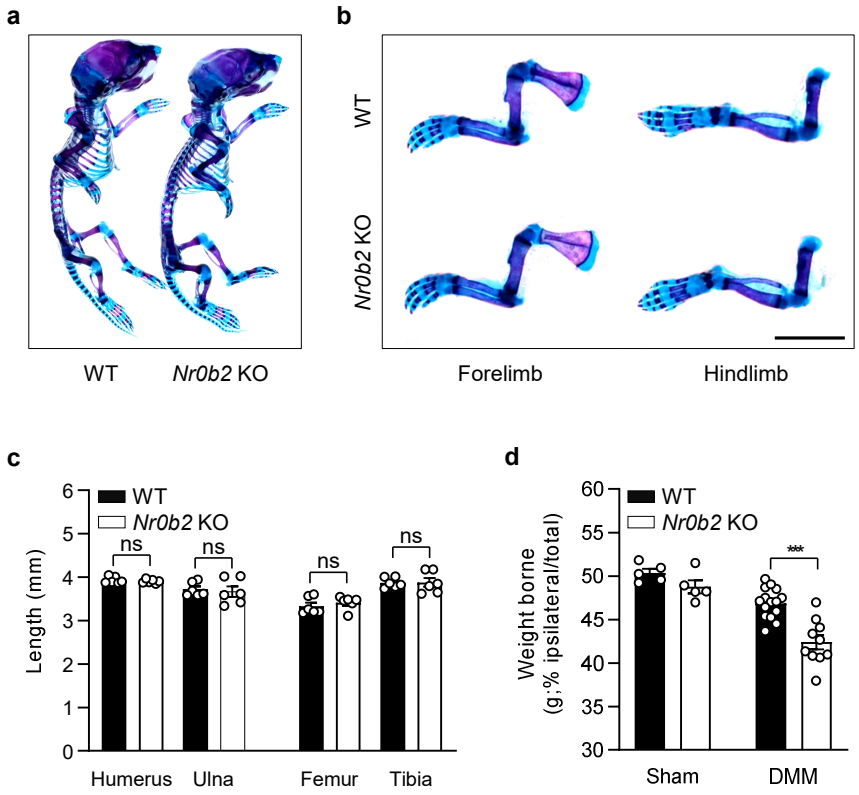

Supplementary Fig. 2 Characterization of *Nr0b2* KO mice in skeletal development. a Representative whole-mount skeletal-stained images of WT and *Nr0b2* KO mice at the newborn stage (postnatal day 4). **b, c** Representative skeletal staining (**b**) and measurement of the length of forelimbs (humerus and ulna) and hindlimbs (femur and tibia) (**c**) in WT and *Nr0b2* KO mice at the newborn stage (postnatal day 4) (WT $n = 6$, *Nr0b2* KO $n = 6$ biologically independent mice). Scale bar, 5 mm. **d** The percentage of weight borne on the sham- or DMM-operated ipsilateral hindlimb relative to the total weight borne on the ipsilateral and unoperated contralateral hindlimbs of WT and *Nr0b2* KO mice, as assessed using an incapacitance tester at 4 weeks post-surgery (WT-sham $n = 5$, *Nr0b2* KO-sham $n = 5$, WT-DMM $n = 15$, *Nr0b2* KO-DMM $n = 10$ biologically independent mice). Data are presented as means ± SEMs. Statistical analyses were performed using a two-sided Student's t-test (**c**, **d**) (ns, not statistically significant, $***p < 0.001$). Source data, including the exact *p*-values, are provided as a Source Data file.

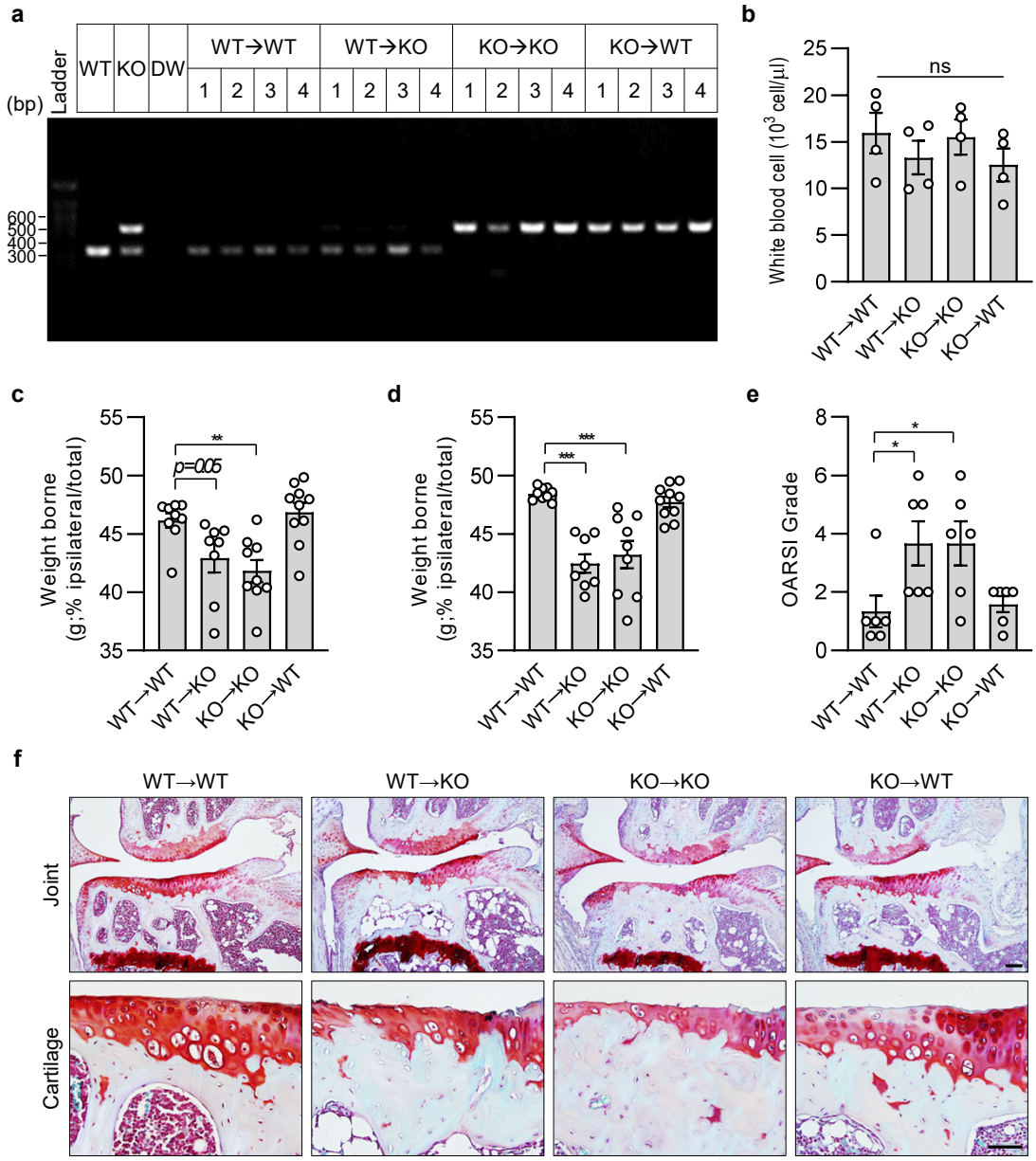

Supplementary Fig. 3 NR0B2 deficiency in joint parenchymal cells increases cartilage destruction in DMM-induced OA. a–f Bone marrow chimeric mice were generated by bone marrow transplantation. WT mice reconstituted with WT bone marrow-derived cells (WT→WT); *Nr0b2* KO mice reconstituted with WT bone marrow-derived cells (WT→KO); *Nr0b2* KO mice reconstituted with *Nr0b2* KO bone marrow-derived cells (KO→KO); WT mice reconstituted with *Nr0b2* KO bone marrow-derived cells (KO→WT). **a, b** Genotype analysis of the *Nr0b2* gene in genomic DNA extracted from peripheral blood of chimeric mice (**a**) and white blood cell counts (**b**) in bone-marrow chimeric mice at 7 weeks after bone marrow transplantation ($n = 4$ biologically independent mice per group). **c–f** Bone marrow chimeric mice received DMM surgery at 8 weeks after bone marrow transplantation. The percentage of weight borne on the DMM-operated ipsilateral hindlimb relative to the total weight borne on the ipsilateral and unoperated contralateral hindlimbs of bone-marrow chimeras, as assessed using an incapacitance tester at 4 weeks (**c**) and 8 weeks (**d**) after surgery (WT→WT $n = 9$, WT→KO $n = 8$, KO→KO $n = 9$, KO→WT $n = 10$ biologically independent mice). Scoring of OARSI grade (**e**) in Safranin-O staining knee joint section and representative Safranin-O staining images (**f**) showing the whole joint and cartilage destruction in the knee joint section from DMM-operated bone marrow chimeric mice at 8 weeks after surgery ($n = 6$ biologically independent mice per group). Images are representative of three independent experiments with similar results. Scale bar, 100 μm for whole joint and 50 μm for cartilage destruction. Data are presented as means ± SEMs. Statistical analyses were performed using a one-way ANOVA, Dunnett's multiple comparisons test (**b**, **c**, **d**, **e**) (ns, not statistically significant, $*p < 0.05$, $**p < 0.01$, and $***p < 0.001$ vs WT→WT). Source data, including the exact *p*-values are provided as a Source Data file. The uncropped agarose gel images are provided in Supplementary Fig. 16.

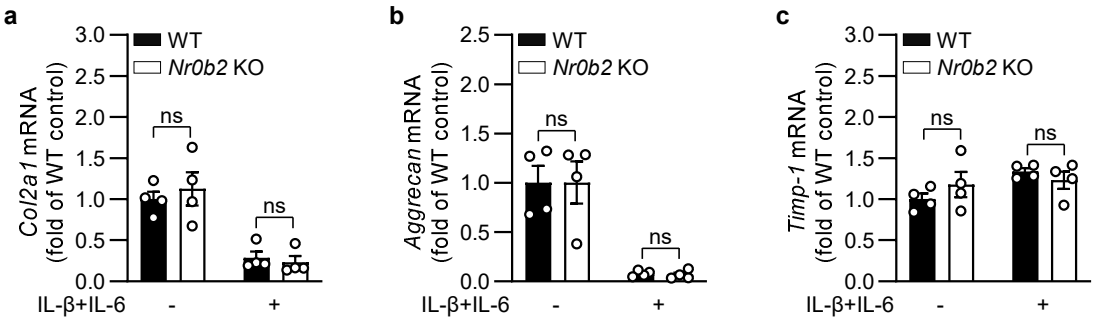

Supplementary Fig. 4 Loss of NR0B2 does not alter the expression of anabolic and anti-catabolic genes in chondrocytes. a–**c** RT-qPCR results showing the relative mRNA expression levels of cartilage anabolic factors *Col2a1* (**a**), *Aggrecan* (**b**), and anti-catabolic factor *Timp-1* (**c**) in primary WT and *Nr0b2* KO mouse chondrocytes after treatment with IL-1β and IL-6 for 24 h (n = 4 per group). Data are presented as means ± SEMs. Statistical analyses were performed using a two-sided Student's t-test (**a**–**c**) (ns, not statistically significant). Source data, including the exact p-values, are provided as a Source Data file.

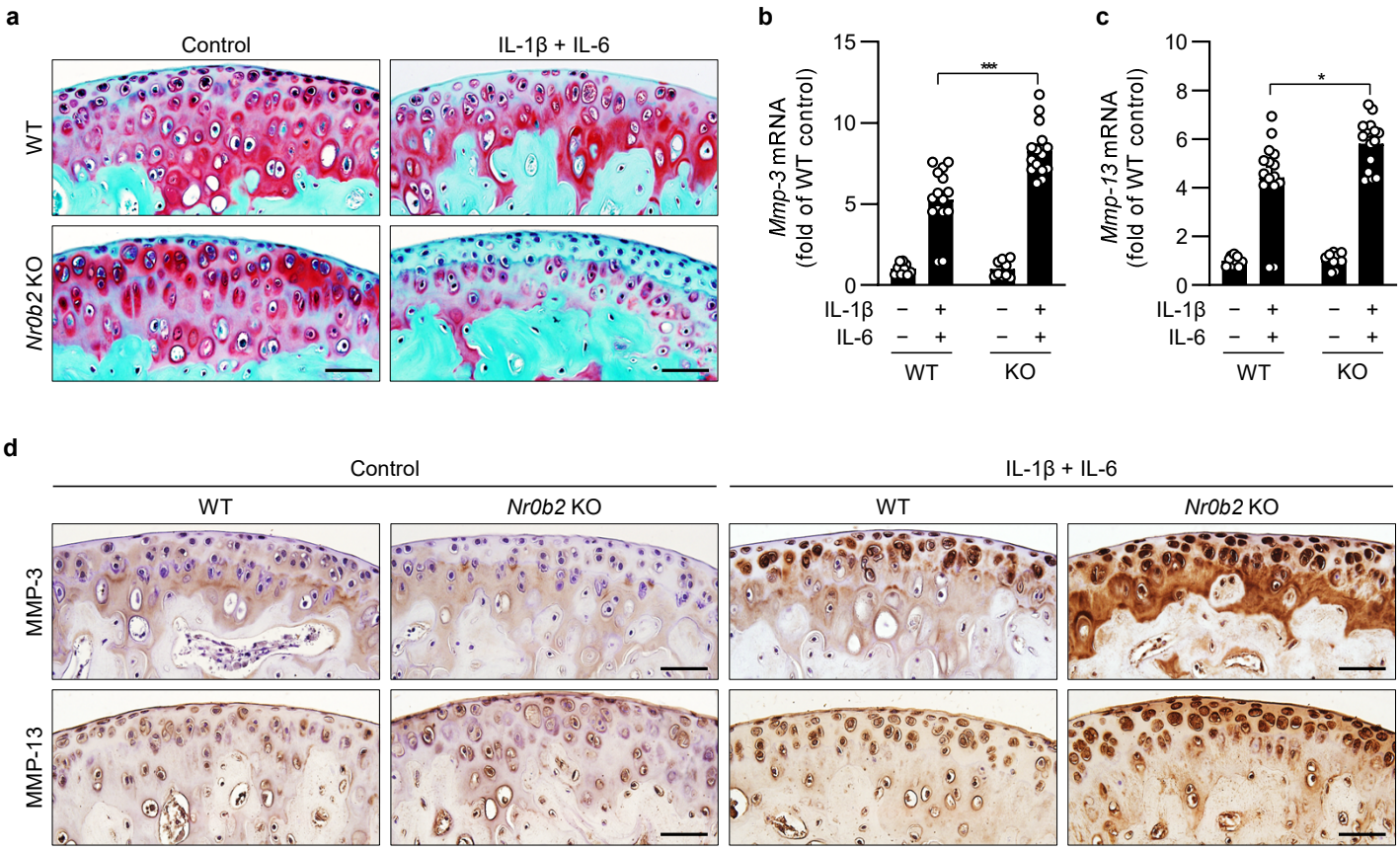

Supplementary Fig. 5 NR0B2 deficiency upregulates expression of MMP-3 and MMP-13 in cartilage explants. a–d Femoral head cartilage explants from WT and *Nr0b2* KO mice were treated with or without IL-1β (10 ng/mL) and IL-6 (100 ng/mL) for 24 h (**b**, **c**) or 72 h (**a**, **d**) and were subjected to Safranin-O staining (**a**), RT-qPCR analysis of relative *Mmp-3* (**b**) and *Mmp-13* (**c**) mRNA levels, and immunostaining for MMP-3 and MMP-13 protein (**d**). Scale bar, 50 μm. (WT-control $n = 9$, WT-IL-1β+IL-6 $n = 15$, *Nr0b2* KO-control $n = 9$, *Nr0b2* KO-IL-1β+IL-6 $n = 15$ biologically independent mice). Data are presented as means ± SEMs. Statistical analyses were performed using a two-sided Student's t-test (**b**, **c**) (*$p < 0.05$ and ***$p < 0.001$). Source data, including the exact *p*-values, are provided as a Source Data file.

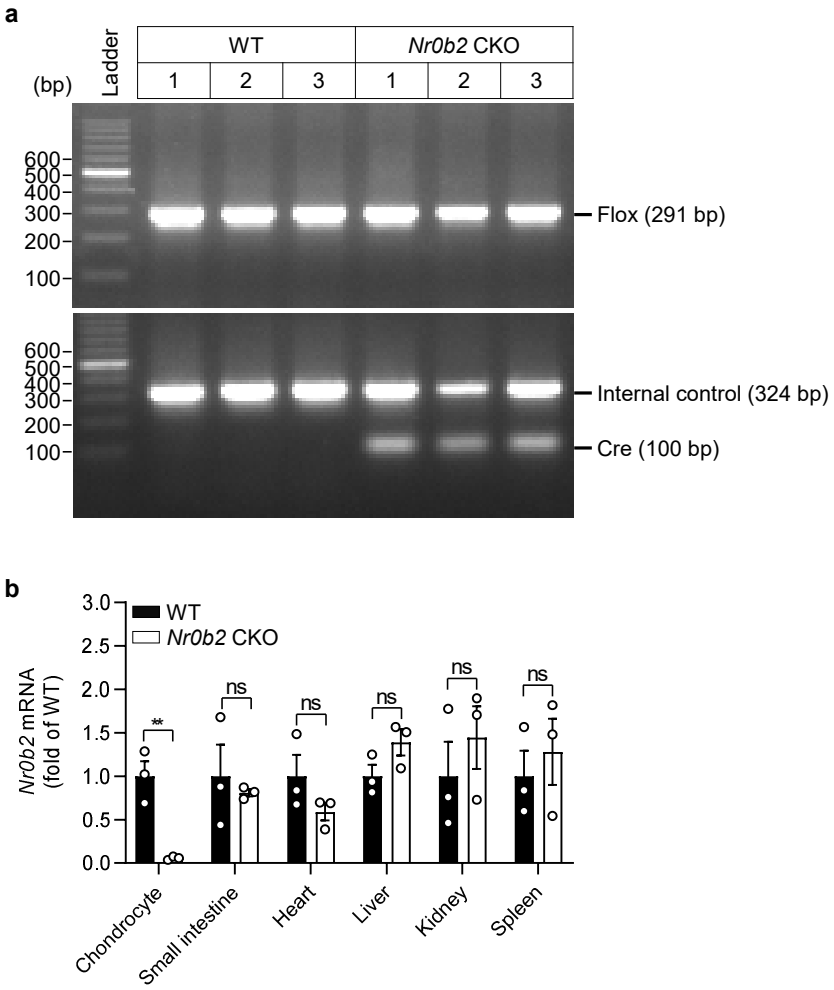

Supplementary Fig. 6 Genotyping of WT and *Nr0b2* CKO mice. a Genotyping of WT and *Nr0b2* CKO mice was performed by PCR and agarose gel electrophoresis. **b** RT-qPCR results showing the relative mRNA expression levels of *Nr0b2* in different tissues of WT and *Nr0b2* CKO mice (n = 3 biologically independent mice per group). Data are presented as means ± SEMs. Statistical analyses were performed using a two-sided Student's t-test (**b**) (ns, not statistically significant, $^{**}p < 0.01$). Source data, including the exact p-values are provided as a Source Data file. The uncropped agarose gel images are provided in Supplementary Fig. 17.

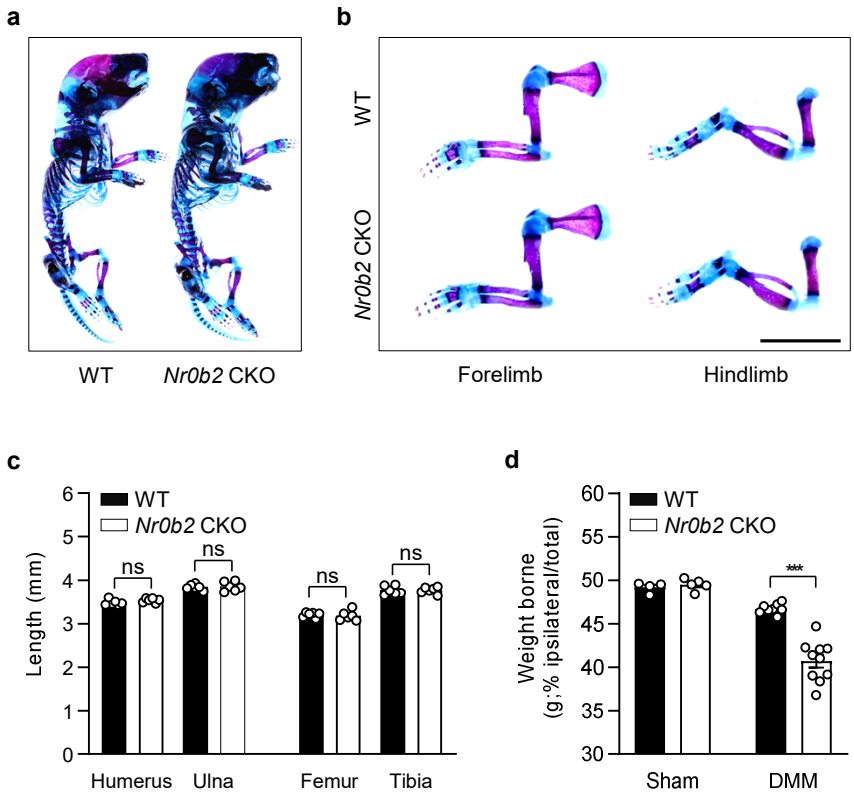

Extended Data Fig. 7 Characterization of *Nr0b2* CKO mice in skeletal development. a Representative whole-mount skeletal-stained images of WT and *Nr0b2* CKO mice at the newborn stage (postnatal day 4). **b, c** Representative skeletal staining (**b**) and measurement of the length of forelimbs (humerus and ulna) and hindlimbs (femur and tibia) (**c**) in WT and *Nr0b2* CKO mice at the newborn stage (postnatal day 4) (WT $n = 6$, *Nr0b2* CKO $n = 6$ biologically independent mice). Scale bar, 5 mm. **d** The percentage of weight borne on the sham- or DMM-operated ipsilateral hindlimb relative to the total weight borne on the ipsilateral and unoperated contralateral hindlimbs of WT and *Nr0b2* CKO mice, as assessed using an incapacitance tester at 4 weeks post-surgery (WT-sham $n = 4$, *Nr0b2* CKO-sham $n = 5$, WT-DMM $n = 8$, *Nr0b2* CKO-DMM $n = 10$ biologically independent mice). Data are presented as means ± SEMs. Statistical analyses were performed using a two-sided Student's t-test (**c**, **d**) (ns, not statistically significant, $***p < 0.001$). Source data, including the exact *p*-values, are provided as a Source Data file.

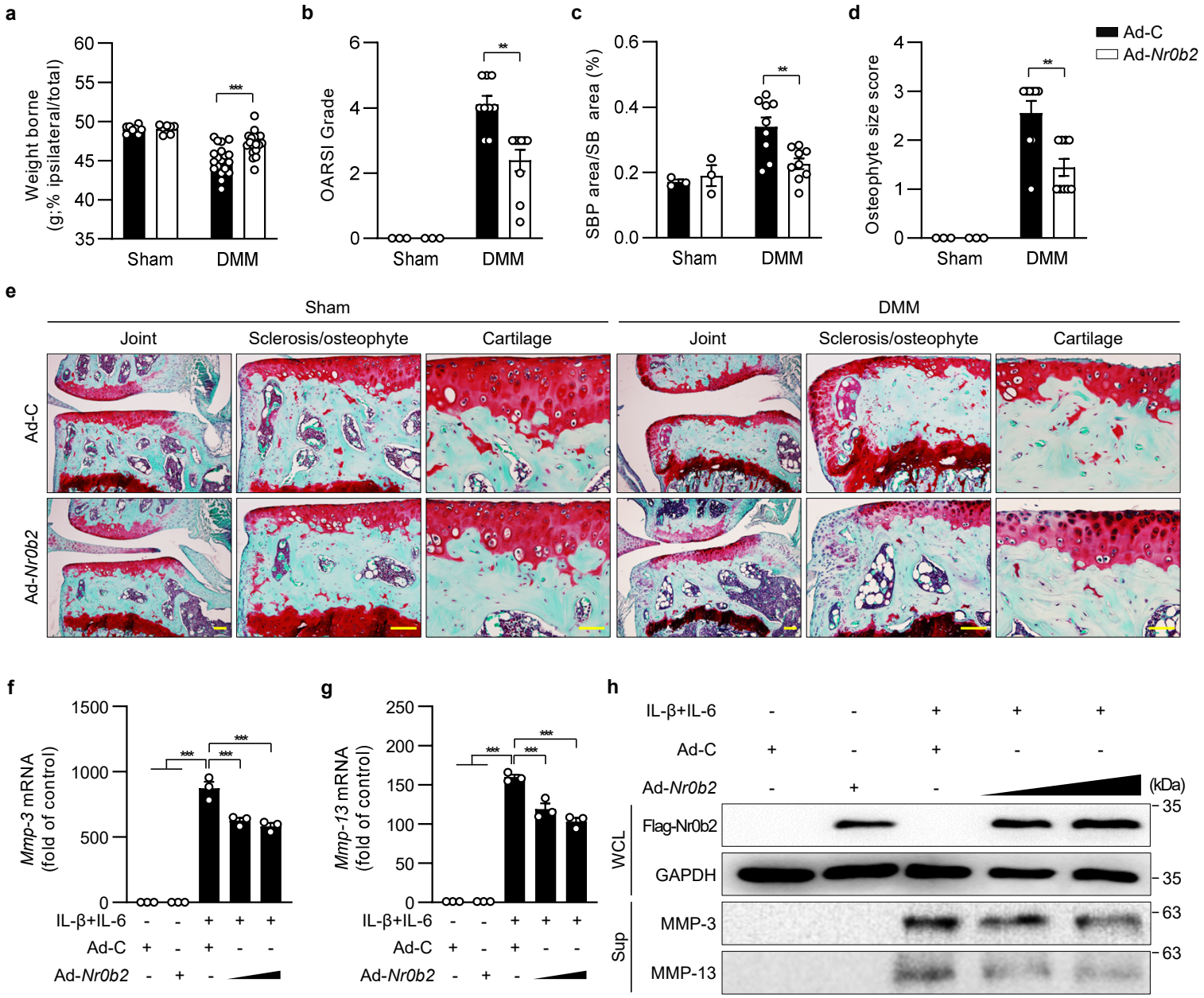

Supplementary Fig. 8 Adenovirus-mediated *Nr0b2* overexpression protects against experimental OA. a–e WT mice were injected intra-articularly with Ad-C or Ad-*Nr0b2* once weekly for 3 weeks after 1 week post-surgery. Mice were sacrificed 8 weeks after DMM surgery. **a** The percentage of weight borne on the sham- or DMM-operated ipsilateral hindlimb relative to the total weight borne on the ipsilateral and unoperated contralateral hindlimbs of WT mice intra-articularly injected with Ad-C or Ad-*Nr0b2*, as assessed using an incapacitance tester at 8 weeks post-surgery (sham-Ad-C $n = 8$, sham-Ad-*Nr0b2* $n = 7$, DMM-Ad-C $n = 19$, DMM-Ad-*Nr0b2* $n = 18$ biologically independent mice). **b–e** Quantitative analysis of OA-related parameters including the OARSI grade for articular cartilage destruction (**b**), the ratio of subchondral bone plate (SBP) area to subchondral bone (SB) area for SB sclerosis (**c**), and the osteophyte size score for osteophyte formation (**d**) in Safranin-O stained knee joint section and representative Safranin-O staining images (**e**) showing the whole joint, subchondral bone sclerosis, osteophyte formation, and cartilage destruction in the knee joints sections from sham- or DMM-operated WT mice intra-articularly injected with Ad-C or Ad-*Nr0b2* at 8 weeks post-surgery (sham-Ad-C $n = 3$, sham-Ad-*Nr0b2* $n = 3$, DMM-Ad-C $n = 9$, DMM-Ad-*Nr0b2* $n = 9$ biologically independent mice). Images are representative of three independent experiments with similar results. Scale bar, 100 μm for whole joint, subchondral bone sclerosis, and osteophyte formation, and 50 μm for cartilage destruction. **f–h** RT-qPCR results showing the relative mRNA expression of *Mmp-3* (**f**) *and Mmp-13* (**g**) and western blot results showing MMP-3 and MMP-13 levels in supernatants (Sup) after treatment with IL-1β and IL-6 for 24 h in primary WT mouse chondrocytes infected with increasing doses of Flag-tagged Ad-*Nr0b2* (**h**) ($n = 3$ per group). Western blot images were the representative image from at least three independent experiments. Statistical analyses were performed using two-sided Student's t-test (**a**, **c**), two-sided Mann–Whitney U test (**b**, **d**), and one-way ANOVA with Dunnett's multiple comparisons test (**f**, **g**) (*$p < 0.05$, **$p < 0.01$, and ***$p < 0.001$). Source data, including the exact *p*-values are provided as a Source Data file. The uncropped western blot images are provided in Supplementary Fig. 18.

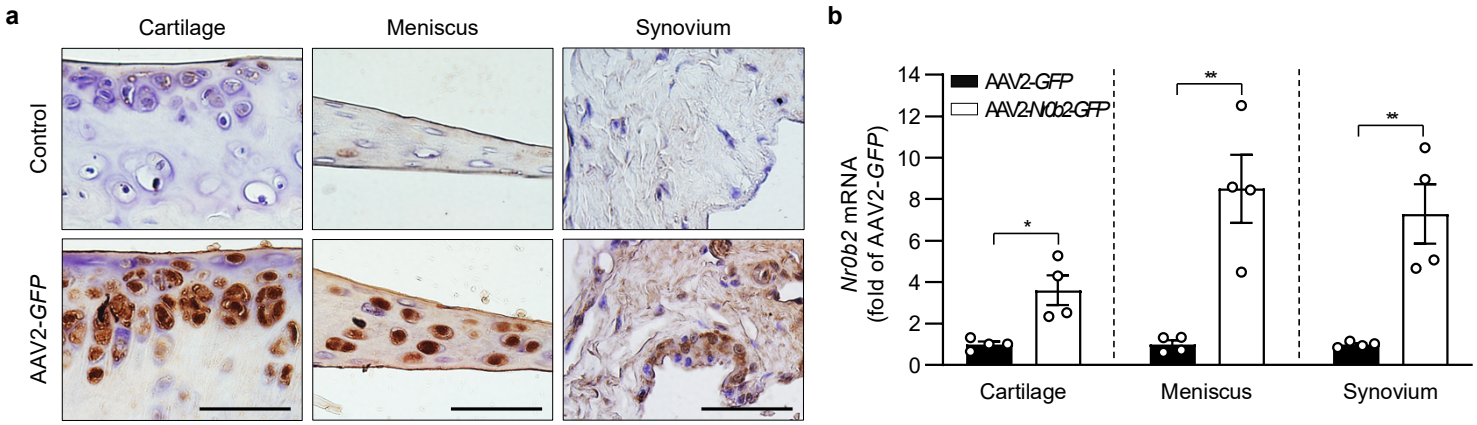

Supplementary Fig. 9 Establishment of NR0B2 overexpression in the mouse knee joint through intra-articular injection of AAV2. a To investigate the infection efficiency of AAV2, representative images of immunostaining for GFP in cartilage, meniscus and synovium of mice 8 weeks after intra-articular injection of vehicle control (PBS) or AAV2-*GFP*. Scale bar, 50 μm. **b** RT-qPCR results showing the relative mRNA expression of *Nr0b2* in the cartilage, meniscus, and synovium of mouse knee joints 2 weeks after intra-articular injection with AAV2-*GFP* or AAV2-*Nr0b2-GFP* (AAV2-*GFP* $n = 4$, AAV2-*Nr0b2-GFP* $n = 4$ biologically independent mice). Data are presented as means ± SEMs. Statistical analyses were performed using a two-sided Student's t-test (**b**) (*$p < 0.05$ and **$p < 0.01$). Source data, including the exact p-values, are provided as a Source Data file.

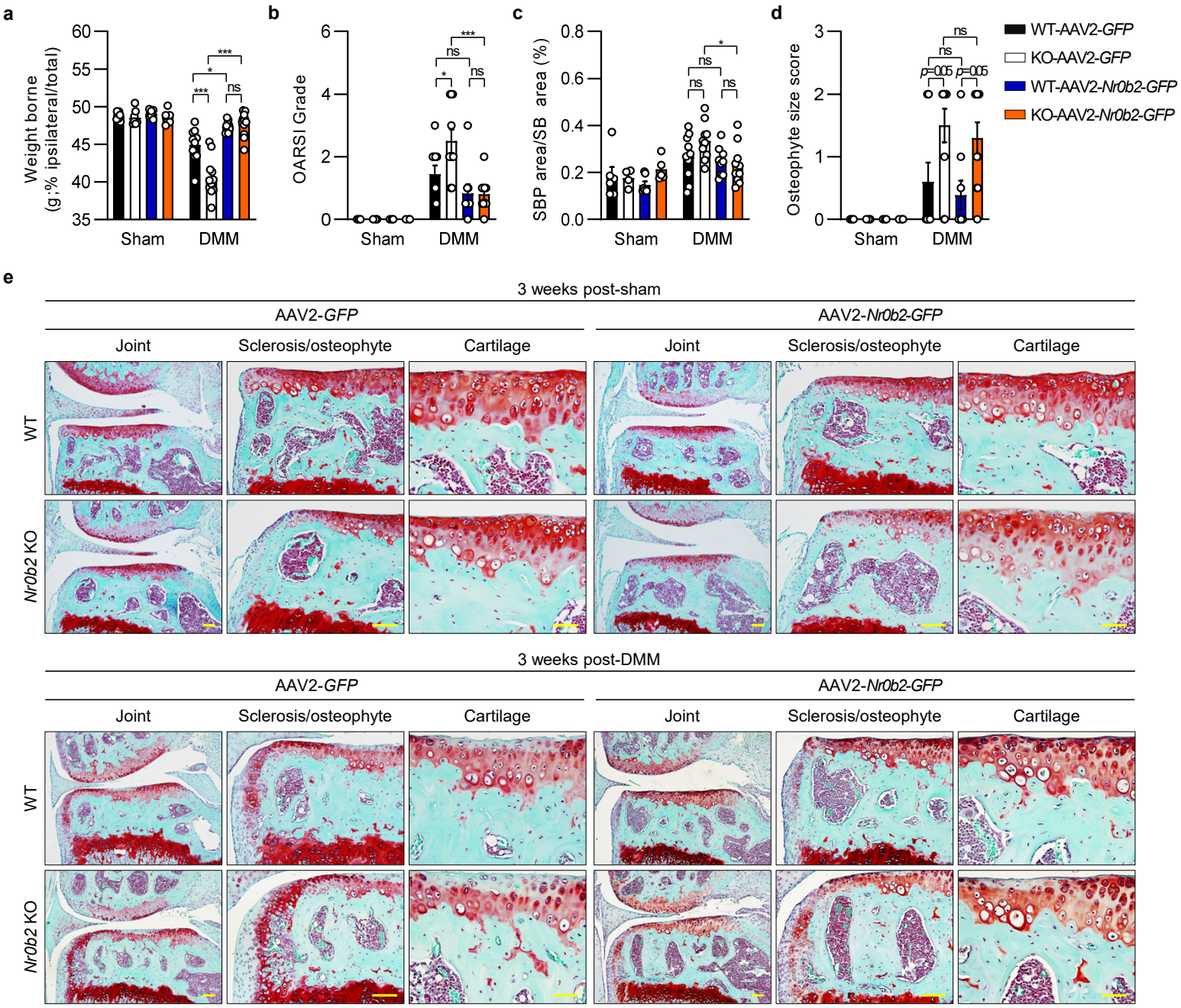

Supplementary Fig. 10 *Nr0b2* delivered by AAV2 protects against the initial stages of DMM-induced OA. a The percentage of weight borne on the sham- or DMM-operated ipsilateral hindlimb relative to the total weight borne on the ipsilateral and unoperated contralateral hindlimbs of WT and *Nr0b2* KO mice intra-articularly injected with AAV2-*GFP* or AAV2-*Nr0b2*-*GFP*, as assessed using an incapacitance tester at 3 weeks post-surgery (WT-sham-AAV2-*GFP* n = 9, *Nr0b2* KO-sham-AAV2-*GFP* n = 7, WT-sham-AAV2-*Nr0b2*-*GFP* n = 10, *Nr0b2* KO-sham-AAV2-*Nr0b2*-*GFP* n = 7, WT-DMM-AAV2-*GFP* n = 10, *Nr0b2* KO-DMM-AAV2-*GFP* n = 11, WT-DMM-AAV2-*GFP* n = 9, *Nr0b2* KO-DMM-AAV2-*Nr0b2*-*GFP* n = 12 biologically independent mice). **b**–**e** Quantitative analysis of OA-related parameters including the OARSI grade for articular cartilage destruction (**b**), the ratio of subchondral bone plate (SBP) area to subchondral bone (SB) area for SB sclerosis (**c**), and the osteophyte size score for osteophyte formation (**d**) in Safranin-O stained knee joint sections and representative Safranin-O staining images (**e**) showing the whole joint, subchondral bone sclerosis, osteophyte formation, and cartilage destruction in the knee joints sections from sham- or DMM-operated WT and *Nr0b2* KO mice intra-articularly injected with AAV2-*GFP* or AAV2-*Nr0b2*-*GFP* at 3 weeks post-surgery (WT sham-AAV2-*GFP* n = 6, *Nr0b2* KO sham-AAV2-*GFP* n = 4, WT sham-AAV2-*Nr0b2*-*GFP* n = 7, *Nr0b2* KO sham-AAV2-*Nr0b2*-*GFP* n = 5, WT DMM-AAV2-*GFP* n = 10, *Nr0b2* KO DMM-AAV2-*GFP* n = 10 WT DMM-AAV2-*Nr0b2*-*GFP* n = 9, *Nr0b2* KO DMM-AAV2-*Nr0b2*-*GFP* n = 10 biologically independent mice). Images are representative of three independent experiments with similar results. Scale bar, 100 μm for whole joint, subchondral bone sclerosis, and osteophyte formation, and 50 μm for cartilage destruction. Data are presented as means ± SEMs. Statistical analyses were performed using a one-way ANOVA, Dunnett's multiple comparisons test (**a**–**d**) (ns, not statistically significant, *$p < 0.05$ and ***$p < 0.001$). Source data, including the exact p-values, are provided as a Source Data file.

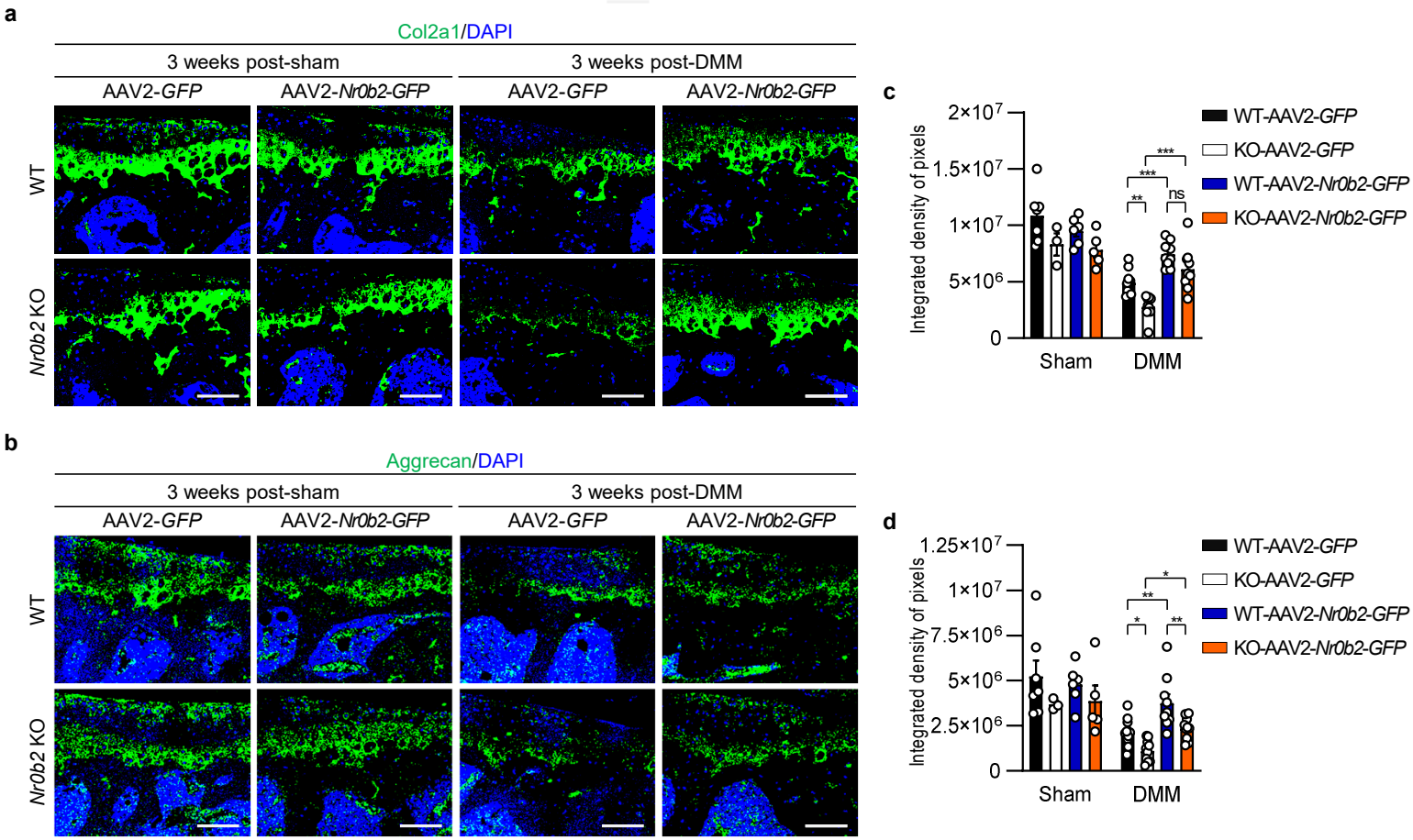

Supplementary Fig. 11 AAV2-mediated delivery of *Nr0b2* attenuates DMM-induced cartilage ECM degradation. a, **b** Representative images of IF staining for Col2a1 (**a**) and Aggrecan (**b**) in the cartilage of knee joint sections from sham- or DMM-operated WT and *Nr0b2* KO mice intra-articularly injected with AAV2-*GFP* or AAV2-*Nr0b2*-*GFP* at 3 weeks post-surgery. Scale bar, 100 μm. **c**, **d** Quantification of integrated density of pixels for Col2a1 (**c**) and Aggrecan (**d**) in the cartilage of knee joint (WT sham-AAV2-*GFP* $n = 7$, *Nr0b2* KO sham-AAV2-*GFP* $n = 3$, WT sham-AAV2-*Nr0b2*-*GFP* $n = 6$, *Nr0b2* KO sham-AAV2-*Nr0b2*-*GFP* $n = 5$, WT DMM-AAV2-*GFP* $n = 10$, *Nr0b2* KO DMM-AAV2-*GFP* $n = 10$, WT DMM-AAV2-*Nr0b2*-*GFP* $n = 9$, *Nr0b2* KO DMM-AAV2-*Nr0b2*-*GFP* $n = 10$ biologically independent mice). Data are presented as means ± SEMs. Statistical analyses were performed using a one-way ANOVA, Dunnett's multiple comparisons test (**c**, **d**) (ns, not statistically significant, $*p < 0.05$, $**p < 0.01$, and $***p < 0.001$). Source data, including the exact *p*-values, are provided as a Source Data file.

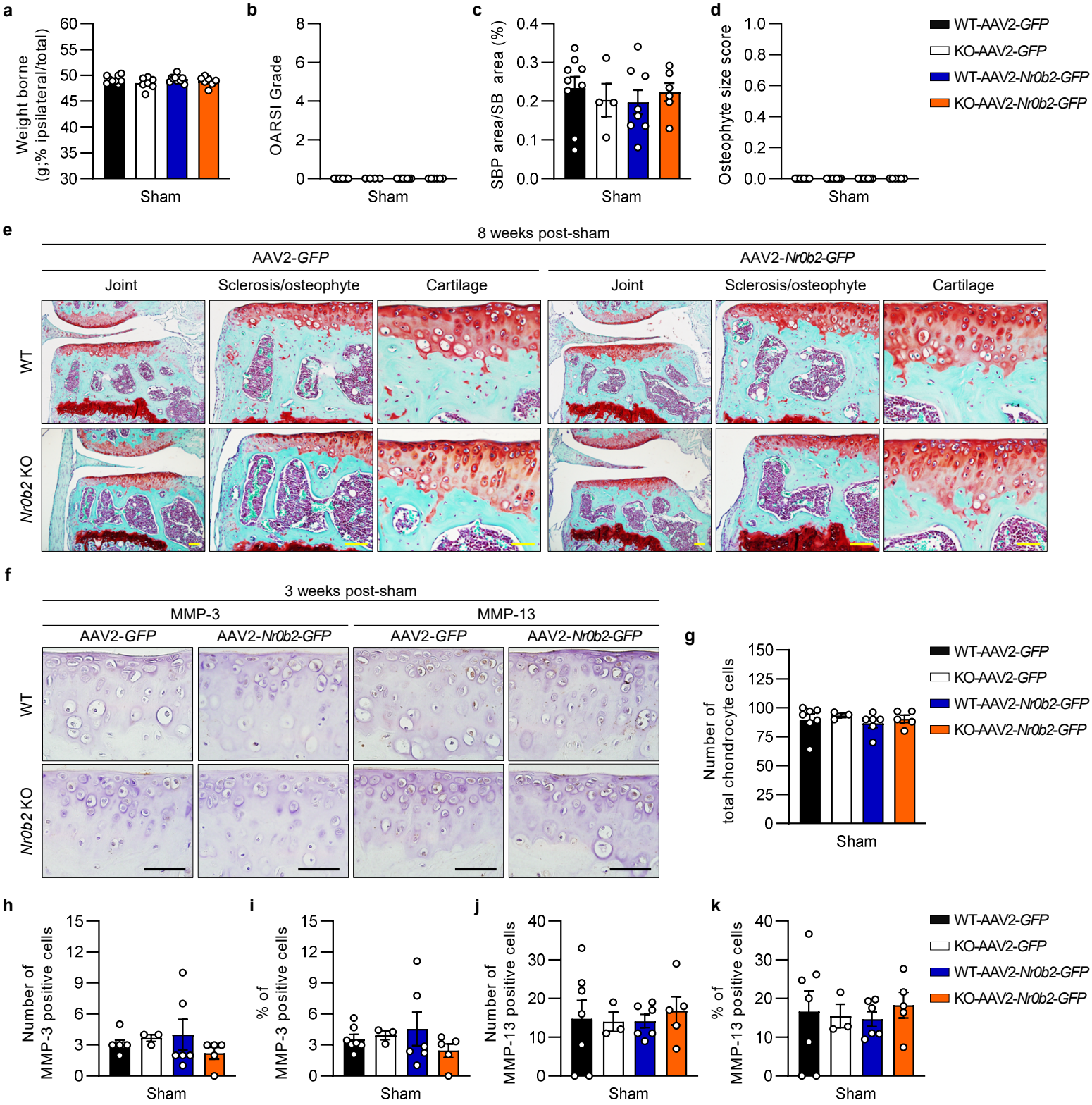
a
Weight borne (g;% ipsilateral/total)
60
55
50
45
40
35
30
Sham
b
OARSI Grade
8
6
4
2
0
Sham
c
SBP area/SB area (%)
0.4
0.3
0.2
0.1
0.0
Sham
d
Osteophyte size score
1.0
0.8
0.6
0.4
0.2
0.0
Sham
WT-AAV2-GFP
KO-AAV2-GFP
WT-AAV2-Nr0b2-GFP
KO-AAV2-Nr0b2-GFP
e
8 weeks post-sham
AAV2-GFP
AAV2-Nr0b2-GFP
Joint
Sclerosis/osteophyte
Cartilage
Joint
Sclerosis/osteophyte
Cartilage
WT
Nr0b2 KO
f
3 weeks post-sham
MMP-3
MMP-13
AAV2-GFP
AAV2-Nr0b2-GFP
AAV2-GFP
AAV2-Nr0b2-GFP
WT
Nr0b2 KO
g
Number of total chondrocyte cells
150
125
100
75
50
25
0
Sham
WT-AAV2-GFP
KO-AAV2-GFP
WT-AAV2-Nr0b2-GFP
KO-AAV2-Nr0b2-GFP
h
Number of MMP-3 positive cells
15
12
9
6
3
0
Sham
i
% of MMP-3 positive cells
15
12
9
6
3
0
Sham
j
Number of MMP-13 positive cells
40
30
20
10
0
Sham
k
% of MMP-13 positive cells
40
30
20
10
0
Sham
WT-AAV2-GFP
KO-AAV2-GFP
WT-AAV2-Nr0b2-GFP
KO-AAV2-Nr0b2-GFP

Supplementary Fig. 12 AAV2-mediated delivery of *Nr0b2* does not have obvious effects on the knee joints of sham mice. a The percentage of weight borne on the sham-operated ipsilateral hindlimb relative to the total weight borne on the ipsilateral and unoperated contralateral hindlimbs of WT and *Nr0b2* KO mice intra-articularly injected with AAV2-*GFP* or AAV2-*Nr0b2*-*GFP*, as assessed using an incapacitance tester at 8 weeks post-surgery (WT-sham-AAV2-*GFP* n = 9, *Nr0b2* KO-sham-AAV2-*GFP* n = 7, WT-sham-AAV2-*Nr0b2*-*GFP* n = 10, *Nr0b2* KO-sham-AAV2-*Nr0b2*-*GFP* n = 7 biologically independent mice). **b**–**e** Quantitative analysis of OA-related parameters including the OARSI grade for articular cartilage destruction (**b**), the ratio of subchondral bone plate (SBP) area to subchondral bone (SB) area for SB sclerosis (**c**), and the osteophyte size score for osteophyte formation (**d**) in Safranin-O stained knee joint sections and representative Safranin-O staining images (**e**) showing the whole joint, subchondral bone sclerosis, osteophyte formation, and cartilage destruction in the knee joints sections from sham-operated WT and *Nr0b2* KO mice intra-articularly injected with AAV2-*GFP* or AAV2-*Nr0b2*-*GFP* at 8 weeks post-surgery (WT-AAV2-*GFP* n = 9, *Nr0b2* KO-AAV2-*GFP* n = 4, WT-AAV2-*Nr0b2*-*GFP* n = 8, *Nr0b2* KO-AAV2-*Nr0b2*-*GFP* n = 6 biologically independent mice). Images are representative of three independent experiments with similar results. **f** Representative images of IHC staining for MMP-3 and MMP-13 in the cartilage of knee joint sections from sham-operated WT and *Nr0b2* KO mice intra-articularly injected with AAV2-*GFP* or AAV2-*Nr0b2*-*GFP* at 3 weeks post-surgery. Scale bar, 50 μm. **g**–**k** Quantification of the total chondrocyte number (**g**), the absolute number (**h**) and percentage (**i**) of MMP-3-positive chondrocytes, and the absolute number (**j**) and percentage (**k**) of MMP-13-positive chondrocytes (WT-AAV2-*GFP* n = 7, *Nr0b2* KO-AAV2-*GFP* n = 3, WT-AAV2-*Nr0b2*-*GFP* n = 6, *Nr0b2* KO-AAV2-*Nr0b2*-*GFP* n = 5 biologically independent mice). Data are presented as means ± SEMs. Statistical analyses were performed using a one-way ANOVA, Dunnett's multiple comparisons test (**a**–**d, g**–**k**) (ns, not statistically significant). Source data, including the exact p-values, are provided as a Source Data file.

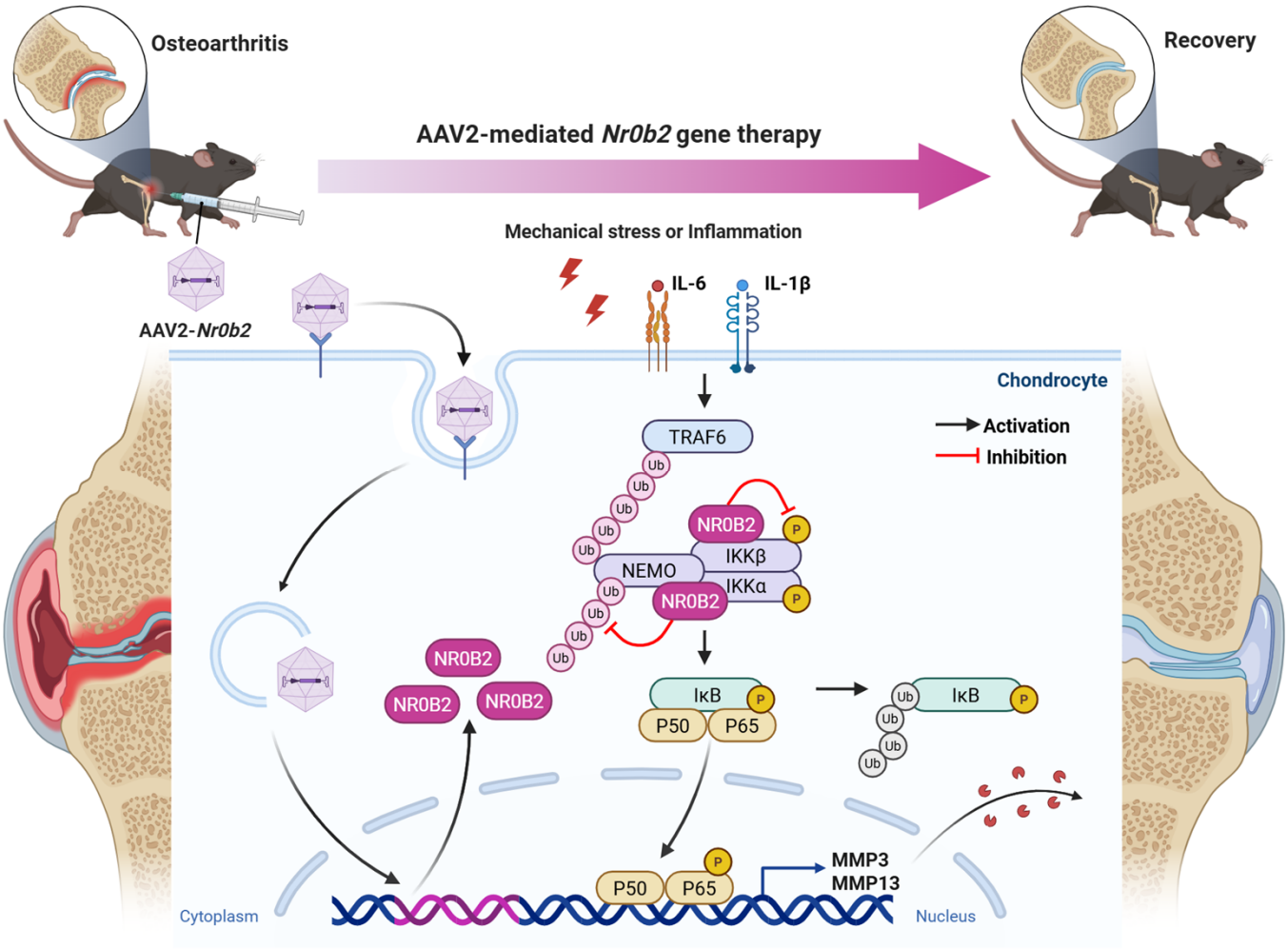

Supplementary Fig. 13 Schematic diagram representing the chondroprotective role of NR0B2 in OA progression. NR0B2 expression is downregulated in the cartilage of human OA patients. Chondrocyte-specific *Nr0b2* deficiency in mice exacerbates DMM-induced experimental OA, accompanied by increased NF-κB-mediated MMP-3 and MMP-13 expression in chondrocytes. Conversely, adeno-associated virus serotype 2 (AAV2)-mediated *Nr0b2* overexpression in the knee joints of mice protects against accelerated knee OA caused by *Nr0b2* deficiency. Mechanistically, NR0B2 regulates the expression of cartilage-degrading enzymes, specifically MMP-3 and MMP-13, by inhibiting IKKβ kinase activity and NEMO ubiquitination through interaction with the components of the IKK complex, resulting in the downregulation of NF-κB signalling. The illustration was created with BioRender.com and has been granted a publication license.

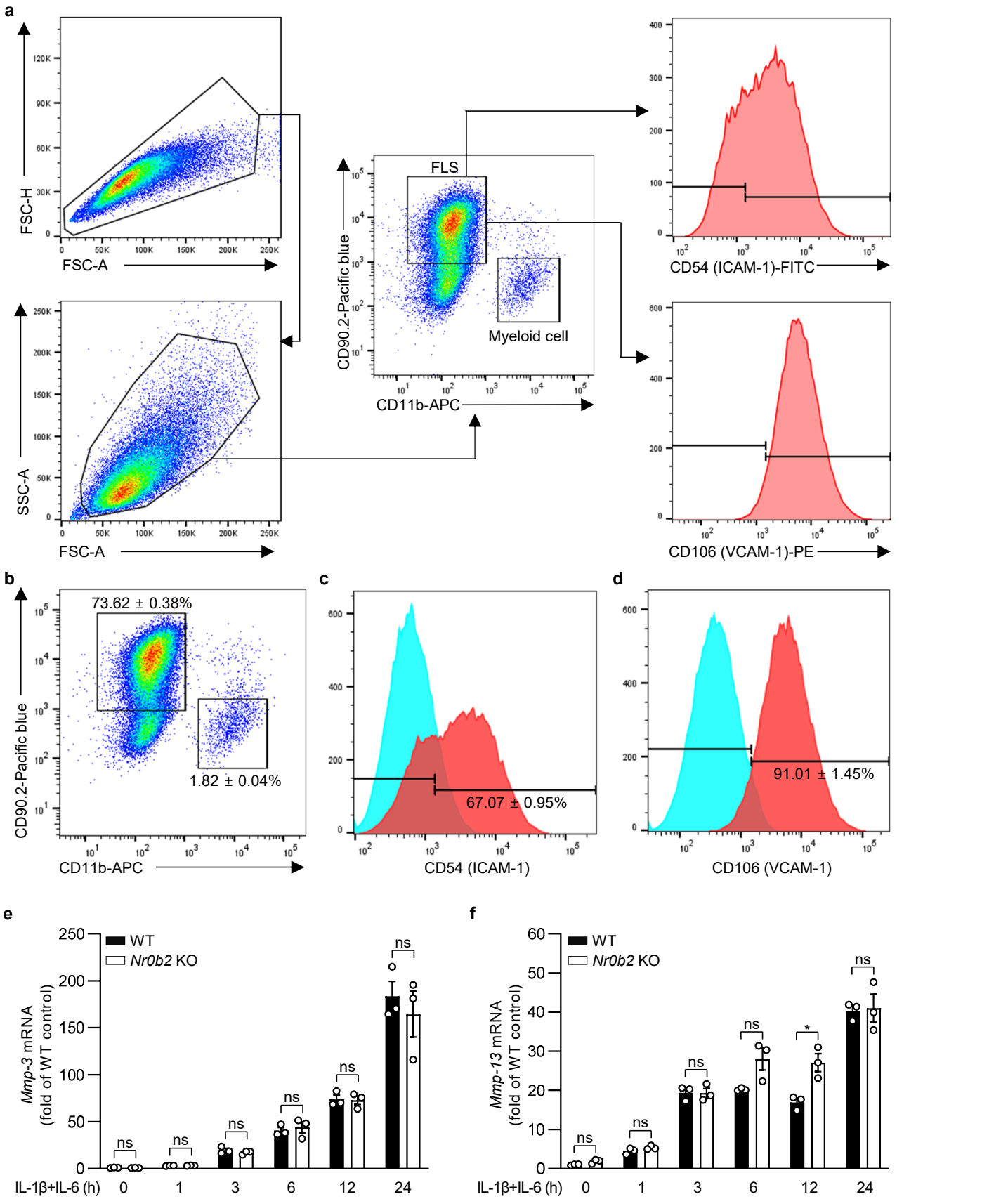

Supplementary Fig. 14 Loss of NR0B2 does not alter the expression of *Mmp-3* and *Mmp-13* in FLS. a–d Isolated FLS from WT and *Nr0b2* KO mice were subjected to flow cytometry analysis on passage 4 after seeding to verify purity. Flow cytometry gating strategy for FLS (**a**). Density plot showing expression of CD90.2 on the majority of the isolated cells (73.62 ± 0.38%) whereas very few CD11b positive myeloid cells can be detected (1.82 ± 0.04%) (**b**). Overlaid histogram showing VCAM-1 expression (red shaded area) on FLS compared to unstained control (blue shaded area) (**c**). Overlaid histogram showing ICAM-1 expression (red shaded area) on FLS or unstained control (blue shaded area) (**d**). **e**, **f** RT-qPCR results showing the relative mRNA expression of *Mmp-3* (**e**) and *Mmp-13* (**f**) in primary FLS isolated from WT and *Nr0b2* KO mice at the indicated time points after treatment with IL-1β and IL-6 (n = 3 per group). Data are presented as means ± SEMs. Statistical analyses were performed using a two-sided Student's t-test (**e**, **f**) (ns, not statistically significant). Source data, including the exact p-values, are provided as a Source Data file.

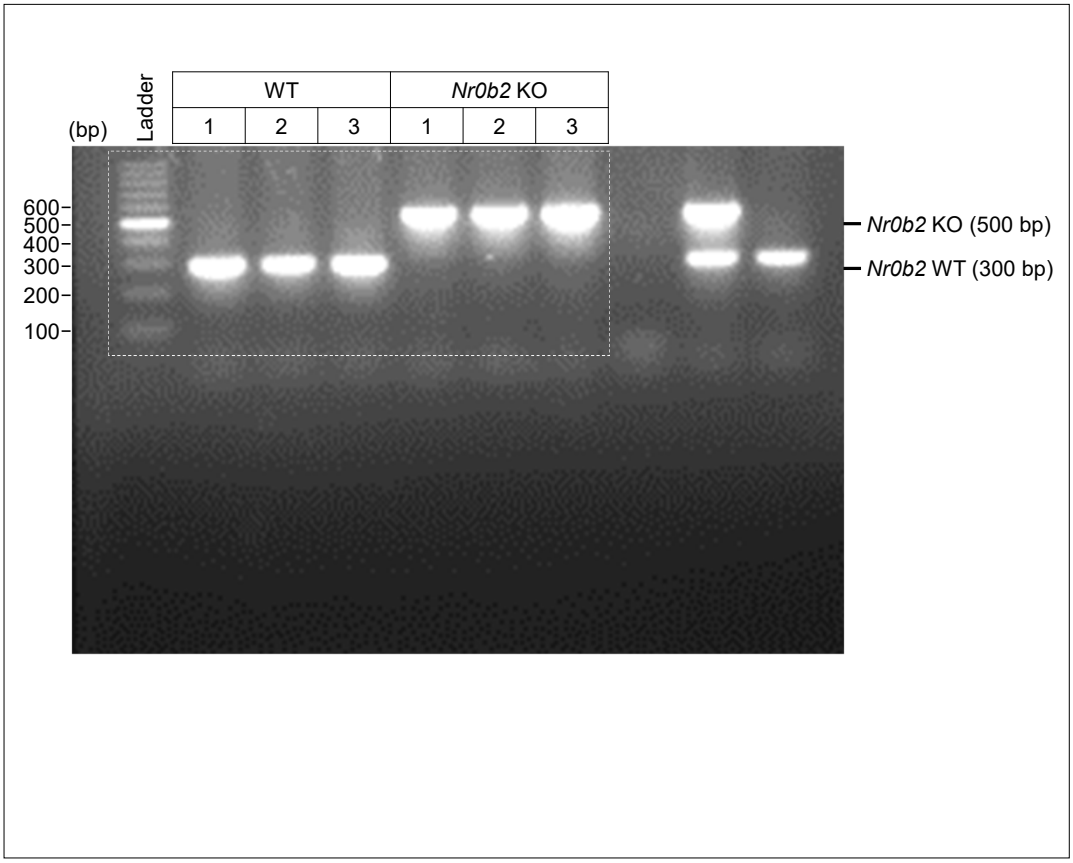

Supplementary Fig. 15 The uncropped agarose gel images presented in the Supplementary Fig. 1a

Note: White dashed lines identify the cropped areas

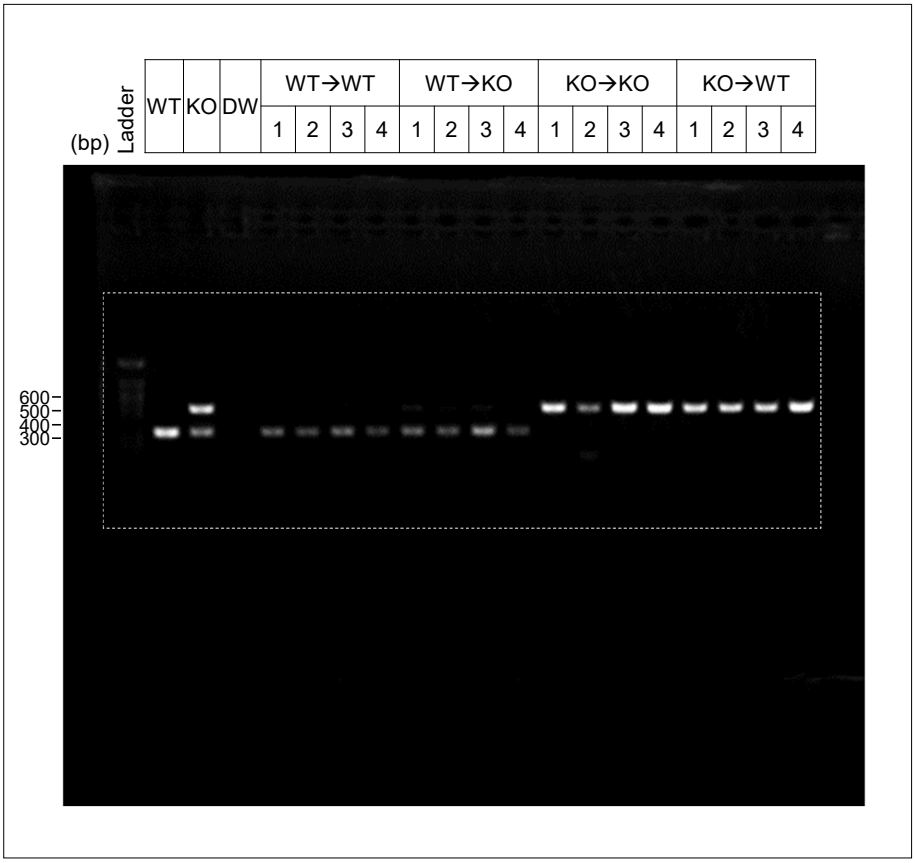

Supplementary Fig. 16 The uncropped agarose gel images presented in the Supplementary Fig. 3a

Note: White dashed lines identify the cropped areas

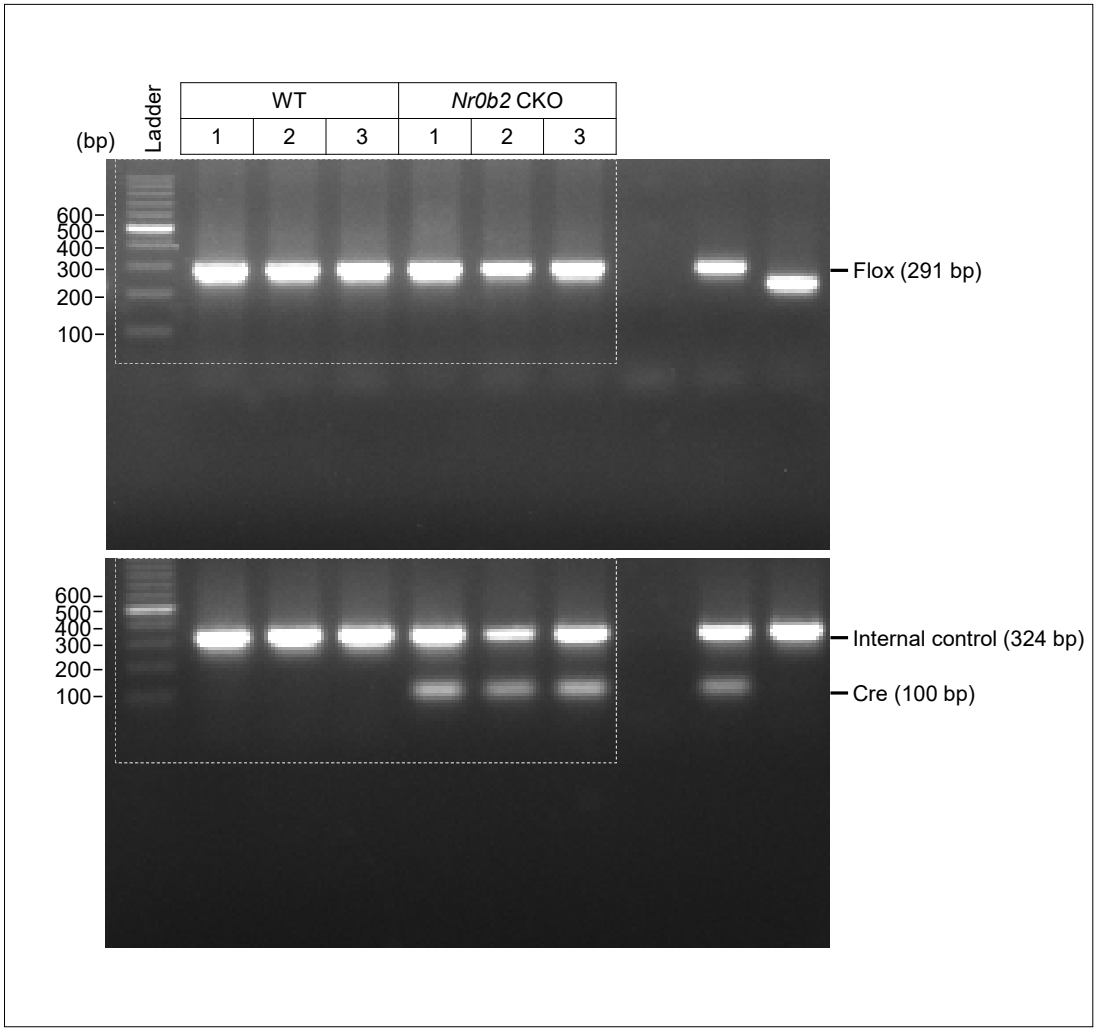

Supplementary Fig. 17 The uncropped agarose gel images presented in the Supplementary Fig. 6a

Note: White dashed lines identify the cropped areas

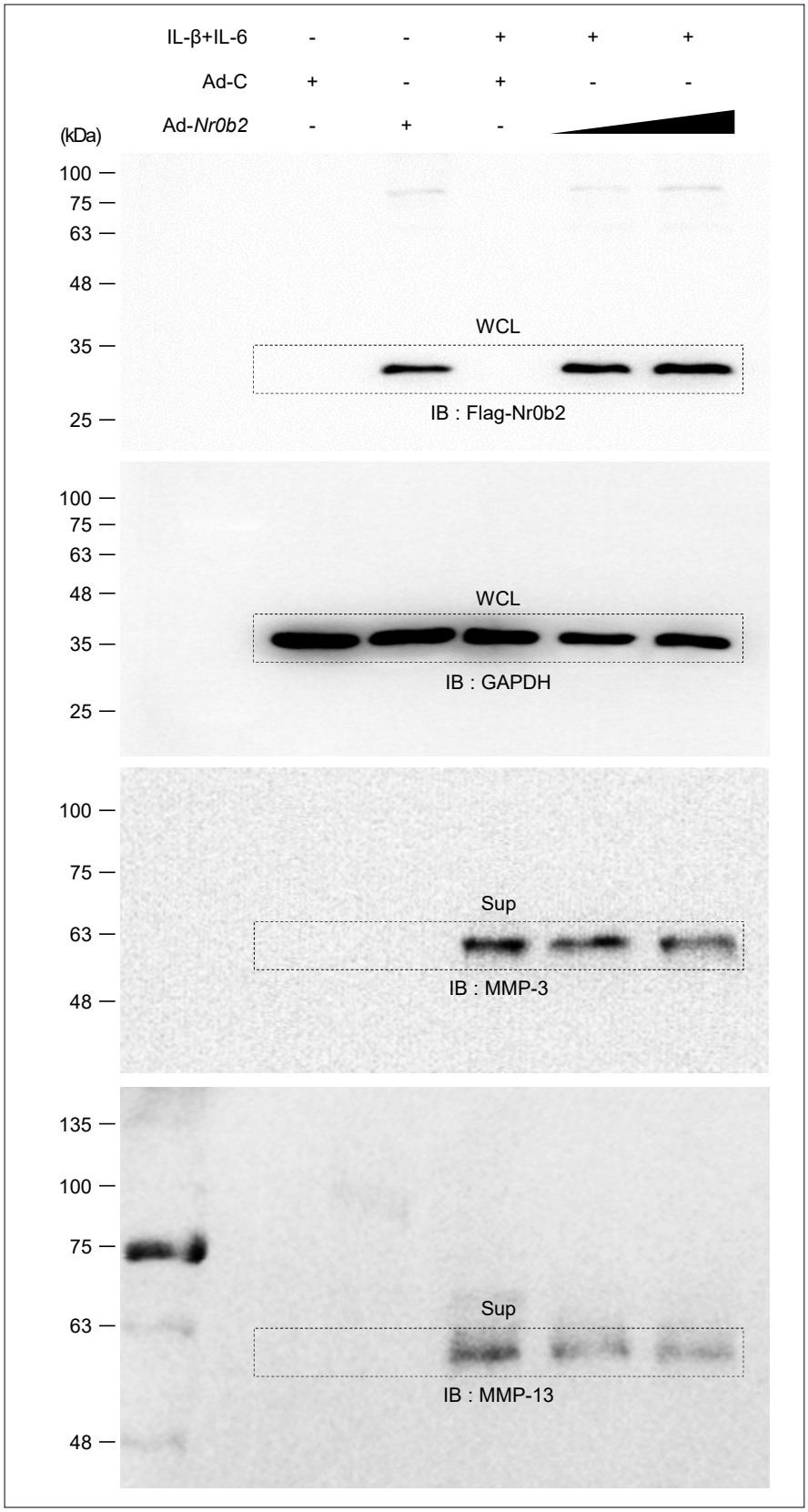

Supplementary Fig. 18 The uncropped western blot images presented in the Supplementary Fig. 8h

Note: Black dashed lines identify the cropped areas

Supplementary Table 1. OARSI osteoarthritis cartilage histopathology scoring system in mouse.

Grade	Osteoarthritic damage
0	Normal
0.5	Loss of Safranin-O without structural changes
1	Small fibrillations without loss of cartilage
2	Vertical clefts down to the layer immediately below the superficial layer and some loss of surface lamina
3	Vertical clefts/erosion to the calcified cartilage extending to <25% of the articular surface
4	Vertical clefts/erosion to the calcified cartilage extending to 25–50% of the articular surface
5	Vertical clefts/erosion to the calcified cartilage extending to 50–75% of the articular surface
6	Vertical clefts/erosion to the calcified cartilage extending >75% of the articular surface

Supplementary Table 2. Assessment of osteophyte size in mouse knee joints.

Grade	Features
0	None
1	Small (approx. Same thickness as the adjacent cartilage)
2	Medium (approx. 1–3 times the thickness of the adjacent cartilage)
3	Large (approx. >3 times the thickness of the adjacent cartilage)

Supplementary Table 3. List of antibodies used in this study.

Name of Antibody	Catalog No.	Company	Dilution used
Flag-tag	ab205606	Abcam	1:1000 WB
HA-tag	H6908	Sigma-Aldrich	1:1000 WB
Strep-tag	34850	QIAGEN	1:3000 WB
p-IKKα/β (Ser180/Ser181)	PA5-36718	Invitrogen	1:1000 WB
p-IκBα (Ser32/36)	9246S	Cell Signaling Technology	1:1000 WB
p-NF-κB p65	3033S	Cell Signaling Technology	1:1000 WB
p-NF-κB p65	ab86299	Abcam	1:100 IHC
NF-κB p65	8242S	Cell Signaling Technology	1:1000 WB, 1:200 IF
IKKα	sc7606	Santa Cruz	1:1000 WB
IKKβ (D30C6)	8943S	Cell Signaling Technology	1:1000 WB
IKKγ (FL-419)	sc-8330	Santa Cruz	1:1000 WB
Ubiquitin (P4D1)	sc-8017	Santa Cruz	1:500 WB
α-tubulin	2144S	Cell Signaling Technology	1:1000 WB
Lamin B (C-20)	sc-6216	Santa Cruz	1:1000 WB
GAPDH	2118S	Cell Signaling Technology	1:1000 WB
β-Actin	4967S	Cell Signaling Technology	1:1000 WB
MMP-13	ARP56350_P050	Aviva	1:1000 WB
MMP-13	ab39012	Abcam	1:1000 WB, 1:200 IHC
MMP-3	ab52915	Abcam	1:1000 WB, 1:200 IHC
GFP	ab290	Abcam	1:500 IHC
SHP (H-5)	sc-271511	Santa Cruz	1:50 IHC
COL2A1	MAB8887	Sigma Aldrich	1:100 IF
Aggrecan	AB1031	Sigma Aldrich	1:50 IF
Western blot (WB), Immunofluorescence (IF), Immunohistochemistry (IHC)			

Supplementary Table 4. Sequences of RT-qPCR primers used in this study.

Gene	Primer sequence (5′-3′)	
Nr0b2	Forward	TCTGCAGGTCGTCCGACTATT
	Reverse	TGTCTTGGCTAGGACATCCA
Mmp-3	Forward	GCCATCTCTTCCATCCAACA
	Reverse	CCAGGGTGTGAATGCTTTTA
Mmp-13	Forward	GGAGCCACAGATGAGCACAGA
	Reverse	TGAACGCTCGCAGTGAAAAG
Col2a1	Forward	ACCTTGGACGCCATGAAAGT
	Reverse	CGGGAGGTCTTCTGTGATCG
Aggrecan	Forward	CCCAAGCACAGAGGTAAACAG
	Reverse	CTCACATTGCTCCTGGTCTG
Timp-1	Forward	GCGGTGGGTGGATGAGTAAT
	Reverse	GGGCTGCACAGTGGAGAATAA
18s rRNA	Forward	GACACGGACAGGATTGACAGATTGATAG
	Reverse	GTTAGCATGCCAGAGTCTCGTTCGTT